GPS Solutions (2020) 24:80
https://doi.org/10.1007/s10291-020-00993-0

ORIGINAL ARTICLE

# High-rate Doppler-aided cycle slip detection and repair method for low-cost single-frequency receivers

Jiaojiao Zhao[1,2,3] · Manuel Hernández-Pajares[3,4] · Zishen Li[1] · Liang Wang[1] · Hong Yuan[1]

Received: 25 October 2019 / Accepted: 27 May 2020 / Published online: 8 June 2020


## Abstract

Carrier phase cycle slips can be an important source of error in precise Global Navigation Satellite System (GNSS) positioning. In such cases, cycle slips can seriously compromise the positioning accuracy and reliability, especially for single-frequency receivers, which do not provide simultaneous measurements at different frequencies to generate effective linear combinations for cycle slip detection. We introduce a high-rate Doppler-aided cycle slips detection and repair (DACS-DR) method to detect and repair cycle slips in single-frequency low-cost GNSS receivers, which benefit from the availability of high-rate Doppler measurements. The distributions of the residuals of the time-differenced carrier phase minus the carrier phase change derived from Doppler observations are analyzed systematically under different sampling rates. A comparison is further performed between the low-cost and high-end receivers. Considering that the loss of lock indicator (LLI) output by receivers can also reflect the condition of cycle slips, the reliability of the LLI is also discussed based on our experimental receiver. Based on these analyses, the DACS-DR method is used in a float-PPP experiment with a data set collected under a difficult situation: a high-latitude urban canyon (Akureyry, northern Iceland, Dec. 2017) with intense ionospheric scintillation. The results demonstrate that the convergence time, positioning errors, and the number of re-convergence events are all significantly reduced with the proposed method. Furthermore, the RMS values of the positioning errors in the horizontal and vertical directions are improved by 44.2% and 21.2%, respectively.

**Keywords** Cycle slip detection and repair · Low-cost single-frequency GNSS receiver · High-rate GNSS data · Doppler-aided

## Introduction

To obtain accurate positioning with Global Navigation Satellite Systems (GNSSs), carrier phase measurements are typically used. One of the main sources of errors in carrier phase positioning is cycle slip, which is generally caused by a temporary loss of lock in the carrier tracking loop of a GNSS receiver. Three sources of cycle slips have been distinguished. First, cycle slips are caused by obstructions of satellite signals due to trees, buildings, bridges, mountains, etc.; this is the most frequent source. Second, cycle slips can originate from a low carrier-to-noise density ratio ($C/N0$) attributable to bad ionospheric conditions, multipath, high receiver dynamics, or low satellite elevation. Third, the receiver software can fail, leading to incorrect signal processing (Hofmann-Wellenhof et al. 2012). Reliable algorithms to identifying and repairing cycle slips are essential.

Some cycle slip detection methods have been proposed and commonly used since the 1980s; examples include the Kalman filtering technique (Bastos and Landau 1988), the TurboEdit method (Blewitt 1990; Bisnath and Langley 2000), the polynomial fitting method (Lichtenegger and Hofmann-Wellenhof 1990), the higher-order time difference method (Kleusberg et al. 1993), the Doppler-aided method (Xu and Xu 2007; Dai 2012) and the combined method involving the pseudorange and carrier phase measurements (Collin and Warnant 1995). Moreover, with the

✉ Zishen Li
lizishen@aircas.ac.cn

1 Aerospace Information Research Institute (AIR), Chinese Academy of Sciences, Beijing, China

2 University of Chinese Academy of Sciences, Beijing, China

3 UPC-IonSAT, Universitat Politècnica de Catalunya, Barcelona, Spain

4 IEEC-CTE-CRAE, Institut d'Estudis Espacials de Catalunya, Barcelona, Spain

emergence of triple-frequency signals, some methods utilizing triple-frequency observations have been proposed (Dai et al. 2009; Wu et al. 2010; Zhao et al. 2015; Zhang and Li 2016). Among these methods, the TurboEdit method and the new methods based on triple-frequency observations are not available for single-frequency receivers. In fact, single-frequency observations are usually of poor quality for low-cost receivers in a civilian application, and the corresponding detection and repair of cycle slips are more challenging, especially in urban canyon environments where the number of visible satellites can be very significantly reduced. Under these circumstances, the capabilities of detecting and repair cycle slips are more significant for the continuity and reliability of precise positioning, such as precise point positioning (PPP) and continuous real-time kinematic (RTK) (Li et al. 2019). For a single-frequency receiver, the polynomial fitting method judges cycle slips by evaluating the discrepancies between the polynomial and the carrier phase time series, whereas the differencing process in the higher-order time difference method amplifies noise. Moreover, the combined method involving pseudorange and carrier phase measurements depends completely on the pseudorange measurement precision, which can be compromised by thermal noise, multipath and ionospheric delay. None of these methods can detect and repair small cycle slips (1 cycle) reliably. Furthermore, when applying the Kalman filter method, the statistical parameters are dependent on engineering experience and must be set appropriately to ensure a reliable cycle slip detection performance. In addition, Kirkko-Jaakkola et al. (2009) employed the receiver autonomous integrity monitoring (RAIM) method to deal with cycle slips and other outliers using the single-frequency time difference phase; the results showed that the RAIM method can successfully identify the individual errors but fails in exemplary multiple-outlier cases.

For single-frequency receivers with Doppler observations, a Doppler-aided method is a good option for addressing cycle slips. Doppler measurements quantify the instantaneous change rate of the carrier phase and are very robust, i.e., immune to cycle slips (Banville and Langley 2012). A few studies have been performed in this field over the last decades. Some researchers proposed methods to detect cycle slips with Doppler measurements using 1 Hz data (Cederholm and Plausinaitis 2014; Wang 2019); unfortunately, these methods cannot repair the cycle slips reliably due to high levels of noise at such sampling rate. Consequently, considering that an increase in the sampling rate can reduce the error using Doppler measurements to predict the carrier phase, it is necessary to study the applications of the Doppler-aided method with high-rate data. Ren et al. (2011) discussed the possibility of detecting and repairing cycle slips with Doppler measurements by conducting a simple analysis of the distribution of residuals from very short-period data with a high-end dual-frequency receiver. Carcanague (2012) provided a detailed analysis of residuals with a Doppler-aided cycle slip detection and repair technique and simulated the performance with 1 Hz and 4 Hz data based on a geometry-based model; nevertheless, the success rate of repairing cycle slips was not high in a semi-urban environment. In addition, Hernández-Pajares et al. (2018) presented a distribution of the residuals with a set of 5 Hz data; the result showed clusters around multiple wavelengths. From the above, we can conclude that the techniques devised to date are still suboptimal, especially for the repair of cycle slips, and thus, further research is needed for low-cost single-frequency receivers with high-rate observations. In consideration of the extensive usage and broad market share of such receivers, a systematic analysis of how low-cost single-frequency receivers could benefit from high-rate Doppler measurements in the detection and repair of cycle slips is needed. This analysis should include by a large number of measurements, and the positioning performance should be analyzed under a real frequent cycle slips situation.

Herein, we focus on a geometry-free method to correctly detect and repair cycle slips using high-rate Doppler measurements with an existing single-frequency low-cost receiver. First, the high-rate Doppler-aided cycle slips detection and repair method for single-frequency receivers is presented in detail. Then, the residuals of the time-differenced carrier phase minus the carrier phase change derived from Doppler observations at different sampling rates are analyzed based on the millions of observations selected for the experiment. A comparison between low-cost and high-end receivers is also performed. Considering that the loss of lock indicator (LLI) information provided by receivers can also reflect the cycle slip condition (IGS 2015), the reliability of the LLI is also evaluated with our experimental receiver based on a real data set with frequent cycle slips. Based on these analyses, the performance of the proposed method is investigated in a float-PPP positioning experiment with data collected under challenging high-latitude urban canyon conditions.

## Methodology

A carrier phase observation in units of length can be expressed as:

$$L^i(k) = \rho_k^i + c \cdot (t_k - t_k^i) - I_k^i + T_k^i + b_k - b_k^i + \lambda \cdot N_k^i + w_k^i + \varepsilon_{L^i(k)} \quad (1)$$

here $\rho_k^i$ is the distance from the receiver to satellite $i$ at epoch $k$, $t_k$ and $t_k^i$ represent the clock biases associated with the receiver and satellite, $c$ is the speed of light. $I_k^i$ and $T_k^i$ are the delays due to the ionosphere and troposphere, respectively, $b_k$ and $b_k^i$ are the receiver and satellite hardware biases, respectively, $\lambda$ is the corresponding signal wavelength,$N_k^i$ is

the integer ambiguity value at epoch $k$, $w_k^i$ is the term due to the phase wind-up effect, and $\varepsilon_{L^i(k)}$ is the sum of unmodeled terms considered noise.

Doppler measurements in units of Hz can be expressed as:

$$D^i(k)\cdot\lambda=\dot{\rho}_k^i+c\cdot(\dot{t}_k-\dot{t}_k^i)-\dot{I}_k^i+\dot{T}_k^i+\dot{w}_k^i+\varepsilon_{D^i(k)} \tag{2}$$

where $\varepsilon_{D^i(k)}$ is the sum of unmodeled terms considered noise, the dot operator on top of the symbols denotes the rate of change of the corresponding magnitude. It should be mentioned that the wind-up effect varies slowly with time for static receivers (Chen et al. 2009).

Carrier phase observations are computed at the receiver by continuously integrating the Doppler frequency shift (Hernández-Pajares et al. 2011). The difference of carrier phase measurements between two consecutive epochs can be described as:

$$\delta L^i=L^i(k)-L^i(k-1)=\lambda\cdot\int_{k-1}^{k}\Delta f\,\mathrm{d}t \tag{3}$$

where $\Delta f$ is the instantaneous Doppler frequency between the receiver and satellite in units of frequency.

Doppler observations provide an instantaneous measure of the change of $\Delta f$ relative to nominal frequency. If no carrier phase cycle slip occurs between two successive epochs, and if the various terms in (1) that depend on the carrier phase can be assumed to vary linearly with time between very close time epochs, $\delta L^i$ can be written approximately as:

$$\delta L^i=L^i(k)-L^i(k-1)=\lambda\cdot\int_{k-1}^{k}\Delta f\,\mathrm{d}t\approx\lambda\cdot\frac{D^i(k)+D^i(k-1)}{2}\cdot\Delta t \tag{4}$$

where $\Delta t$ is the time interval between consecutive epochs.

To clearly understand the sources of error, we express the carrier phase change between two consecutive epochs calculated by carrier phase measurements and Doppler measurements in a more specific way:

$$\begin{cases}\delta L^i=L^i(k)-L^i(k-1)=\delta\rho_{k,k-1}+c\cdot(\delta t_{k,k-1}-\delta t_{k,k-1}^i)-\delta I_{k,k-1}^i+\delta T_{k,k-1}^i+\delta w_{k,k-1}^i+\mathrm{CS}^i\cdot\lambda+\varepsilon_{\delta L^i}\\ \delta L_d^i=\lambda\cdot\frac{D^i(k)+D^i(k-1)}{2}\cdot\Delta t=(\bar{\dot{\rho}}_{k,k-1}^i+c\cdot(\bar{\dot{t}}_{k,k-1}-\bar{\dot{t}}_{k,k-1}^i)-\bar{\dot{I}}_{k,k-1}^i+\bar{\dot{T}}_{k,k-1}^i+\bar{\dot{w}}_{k,k-1}^i)\cdot\Delta t+\varepsilon_{\delta L_d^i}\end{cases} \tag{5}$$

where the dash operator on top of the symbols denotes the mean of the consecutive values for the corresponding terms and $\mathrm{CS}^i$ is the integer cycle slip value. Hardware biases are eliminated because they are considered constant between two adjacent epochs. Similar to the equations above, $\varepsilon_{\delta L^i}$ and $\varepsilon_{\delta L_d^i}$ are the sums of the noise of the unmodeled terms.

The difference between $\delta L^i$ and $\delta L_d^i$ can be simply written in the following format:

$$d_{\delta L}^i=\delta L^i-\delta L_d^i=\mathrm{CS}^i\cdot\lambda+\zeta \tag{6}$$

where $\zeta$ represents the difference between carrier-range variation $\delta L^i$ and $\delta L_d^i$ when no cycle slip occurs, which contain the sum of the total unmodeled measurement noise and the sum of approximate model errors for the items in (5). Hereinafter, we refer to the Difference between these two Carrier-range Variations as the DCV residual for the sake of simplicity. If the absolute value of $\zeta$ is small enough, Equation (6) could be used to detect cycle slips when exceeding a threshold T, by:

$$\left|d_{\delta L}^i\right|>T \tag{7}$$

Note that $d_{\delta L}^i$ equals to $\zeta$ when no cycle slip exists, and should typically be smaller than a half-wavelength for a highly efficient cycle slip detection and repair method. The capability of the test using (7) depends on both the threshold $T$ defined by a tolerable false alarm rate and the distribution of $\zeta$. If $\zeta$ is sufficiently small, the number of cycle slips can be estimated precisely with:

$$\mathrm{CS}^i=\left[\frac{\delta L^i-\delta L_d^i}{\lambda_i}\right] \tag{8}$$

$$|\zeta|=\left|\delta L^i-\delta L_d^i-\mathrm{CS}^i\cdot\lambda_i\right|\le T_2 \tag{9}$$

where the square brackets in (8) represent rounding to the nearest integer and the threshold $T_2$ is defined by a tolerable probability of false repair.

Equation (5) demonstrates that the approximate error in $\delta L_d^i$ will decrease as $\Delta t$ decreases. Therefore, a higher sampling rate is helpful for decreasing DCV residuals. In view of this, we systematically analyze the distribution of DCV residuals when no cycle slips occur to investigate how much benefit can be obtained from an increase in the sampling rate of Doppler measurements. Then, the statistical results are used as a reference to determine the threshold in the proposed geometry-free Doppler-aided cycle slips detection and repair method, hereafter referred to as the DACS-DR method for simplicity.

## Experiments and analyses

To validate the performance of the DACS-DR method, the analyses were arranged as follows. First, the distributions of DCV residuals were analyzed under static and kinematic

modes with real data sets. Then, a comparison between low-cost and high-end receivers was performed, and the performance of using the LLI to detect cycle slips was analyzed by comparing this indicator with the DACS-DR method. Based on the findings, a positioning experiment was conducted with a real data set containing frequent cycle slips.

## Performance analysis of DCV residuals

U-blox is one of the most popular mass-market boards implementing a single-frequency GNSS receiver. The single-frequency receiver we used to characterize the presented technique is the Argonaut receiver, which possesses an internal patch antenna and was commercialized by Rokubun S.L. The core module of the receiver is u-blox NEO-M8T, with firmware u-blox 9 and protocol version 27.11. This receiver can support a sampling rate as high as 10 Hz. We investigated the DCV residuals estimated at different sampling rates under static and kinematic modes.

### Static experiment

Static data with sampling rates of 1 Hz, 5 Hz and 10 Hz were collected with our Argonaut receiver to analyze the performance of the DCV residuals, collecting a large number of measurements (198,000, 835,000 and 2,500,000, respectively) in the city of Barcelona, Spain, over several days in April 2019.

To analyze the feasibility of the DACS-DR method introduced above, the distribution of DCV residuals without cycle slips should be studied first. However, it is difficult to ensure that every small cycle slip in our raw carrier phase measurements has been filtered out. We take three actions to ensure the reliability of our results:

1. Choose an open sky environment and a relatively stable period of ionosphere activity to collect the data.
2. Exclude data for which the LLI shows cycle slips;
3. Exclude data that have large cycle slips detected by 3rd-order time difference of carrier phase measurements. We set the threshold as 2 cycles in this experiment.

After following these steps, we analyzed the distribution and statistics of the DCV residuals of the remaining data. The same processing approaches were used for our kinematic experiment in the next section.

Figure 1 displays the relationship of the DCV residuals and carrier-to-noise density ratio ($C/N0$). Evidently, the DCV residuals increase when the value of $C/N0$ decreases. Considering this relation, the distributions of the DCV residuals of data collected at different sampling rates were analyzed with different intervals of $C/N0$. Figure 2 illustrates two examples of the distributions of the DCV residuals

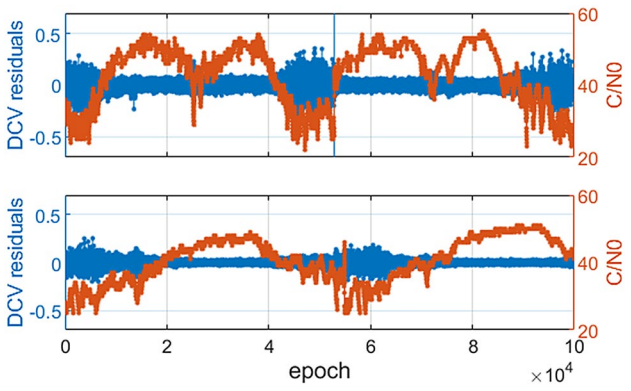


**Fig. 1** Two examples showing the relationships of the DCV residuals (in cycles) and $C/N0$ with the static data collected in April 2019 with the Argonaut receiver (top: G15 at 5 Hz; bottom: G21 at 10 Hz)

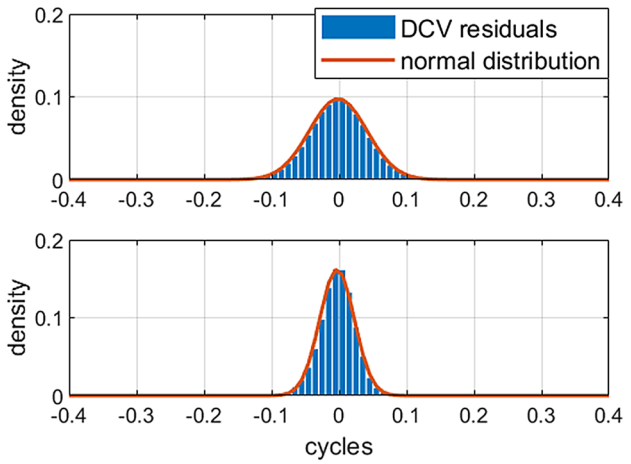


**Fig. 2** Two examples of the distribution of the DCV residuals (in cycles) with 5 Hz data collected in April 2019 with the Argonaut receiver (top: $35 \le C/N0 < 40$; bottom: $C/N0 \ge 45$)

and comparisons with normal distributions. The distributions clearly obey the normal distribution with zero means. The root mean square (RMS) values of the DCV residuals are shown in Table 1, and the corresponding line chart is presented in Fig. 3 for the sake of readability. Evidently, the RMS values of DCV residuals reduce with increasing sampling rate. At the same sampling rate, the RMS values decrease with increasing $C/N0$, while the values are slightly larger at 1 Hz and 5 Hz when $C/N0$ is within the interval of [30, 35]. The reason may lie in the specific processing strategy for the weak signal in the receiver.

For a normal distribution with zero mean, the RMS value is equal to the standard deviation, i.e., sigma value. For the 1 Hz data, the 3 $\sigma$ value is between 0.5 and 1 cycle for most of the DCV residuals. We can conclude that most cycle slips larger than 1 can be correctly detected by the values of DCV residuals. However, detecting small cycle slips of 1 cycle

**Table 1** RMS values of the DCV residuals at different sampling rates and within different *C/N*0 intervals with data collected with the Argonaut receiver (in cycles)

| *C/N*0 | Sampling rate | | |
|---|---|---|---|
| | 1 Hz | 5 Hz | 10 Hz |
| $25 \le C/N0 < 30$ | 0.314 | 0.063 | 0.039 |
| $30 \le C/N0 < 35$ | 0.333 | 0.072 | 0.034 |
| $35 \le C/N0 < 40$ | 0.236 | 0.044 | 0.020 |
| $40 \le C/N0 < 45$ | 0.193 | 0.032 | 0.012 |
| $C/N0 \ge 45$ | 0.159 | 0.026 | 0.009 |

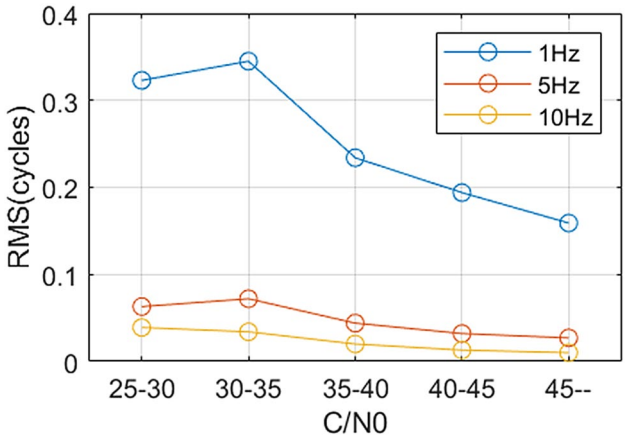


**Fig. 3** RMS values of the DCV residuals of the static data collected with the Argonaut receiver (in cycles)

or repairing the cycle slips correctly with the DACS–DR method is not adequate.

For the 5 Hz and 10 Hz data, all the RMS values of the DCV residuals are smaller than 0.08, indicating with a high likelihood that almost all (more than 99.73%) of the cycle slips can be detected and repaired correctly. This conclusion is considered valuable in real-time precise positioning, which requires long-cycle slip-free arcs of carrier phase measurements (Choy 2011; Wang et al. 2019).

### Kinematic experiment

Kinematic data with sampling rates of 5 and 10 Hz were collected by a driving bus in Barcelona, Spain, with a velocity no greater than 30 m/s to analyze the performance of the DCV residuals. The 5 Hz data were collected on July 1, 2019, from 15:00 to 18:00 (GPST), while the 10 Hz data were collected on July 4, 2019, during the same period. The numbers of measurements in the 5 Hz and 10 Hz data sets are 234,000 and 460,000, respectively. According to Carcanague (2012), the DCV residuals are influenced by the vehicle's velocity, which directly contributes to the Doppler

**Table 2** RMS values of the DCV residuals with different *C/N*0 intervals using the 5 Hz kinematic data collected on July 1, 2019, by the Argonaut receiver (in cycles)

| *C/N*0 | Velocity | | |
|---|---|---|---|
| | < 5 m/s | 5–10 m/s | > 10 m/s |
| $25 \le C/N0 < 30$ | 0.079 | 0.120 | 0.112 |
| $30 \le C/N0 < 35$ | 0.087 | 0.118 | 0.102 |
| $35 \le C/N0 < 40$ | 0.067 | 0.094 | 0.084 |
| $40 \le C/N0 < 45$ | 0.053 | 0.075 | 0.068 |
| $C/N0 \ge 45$ | 0.046 | 0.061 | 0.065 |

**Table 3** RMS values of the DCV residuals with different *C/N*0 intervals using the 10 Hz kinematic data collected on July 4, 2019, by the Argonaut receiver (in cycles)

| *C/N*0 | Velocity | | |
|---|---|---|---|
| | < 5 m/s | 5–10 m/s | > 10 m/s |
| $25 \le C/N0 < 30$ | 0.050 | 0.080 | 0.068 |
| $30 \le C/N0 < 35$ | 0.043 | 0.059 | 0.057 |
| $35 \le C/N0 < 40$ | 0.030 | 0.044 | 0.040 |
| $40 \le C/N0 < 45$ | 0.021 | 0.030 | 0.029 |
| $C/N0 \ge 45$ | 0.018 | 0.022 | 0.022 |

measurements. Thus, the observations were divided into three categories according to the velocity. Table 2 and 3 list the RMS values of the DCV residuals with different *C/N*0 intervals when the sampling rate is 5 Hz and 10 Hz. Figure 4 shows the corresponding line charts for the sake of readability.

According to the results of the kinematic experiment, all the RMS values of the DCV residuals are not larger than 0.12 and 0.08 for 5 Hz and 10 Hz data, respectively. These results demonstrate that almost all cycle slips can be detected and repaired correctly in the kinematic mode with the geometry-free DACS-DR method. Moreover, Fig. 4 illustrates that when the speed is between 5 and 10 m/s, the RMS values are even larger than in situations in which the speed is lower than 5 m/s or higher than 10 m/s. An interpretation is that the vehicle speed increases the frequency of multipath. If the frequency of the multipath exceeds the phase-locked loop (PLL) or frequency-locked loop (FLL) bandwidth, the multipath effects on tracking start to be filtered out (Carcanague 2012).

### Worst-case experiment

To obtain a clear understanding of the DACS-DR method for high-rate data, we performed a worst-case experiment from the perspective of a high expected number of cycle slips in static mode. Data were acquired over approximately 12 h

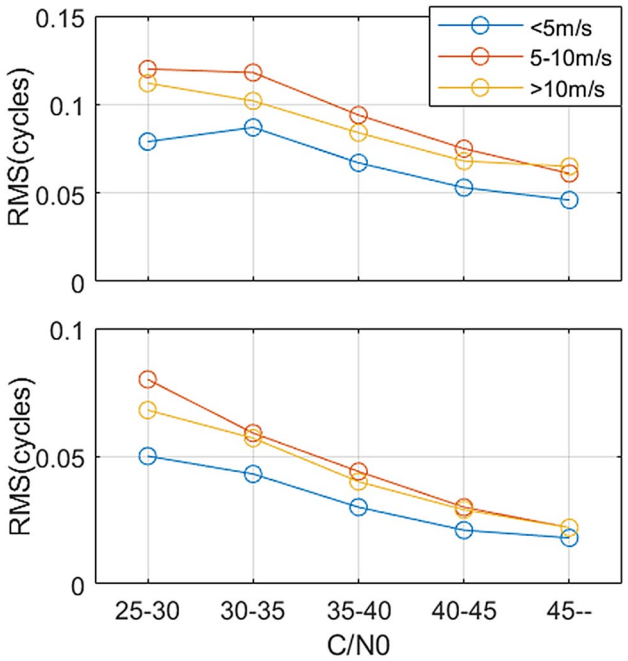


**Fig. 4** RMS values of the DCV residuals with the kinematic data collected with the Argonaut receiver (in cycles; top: 5 Hz, bottom: 10 Hz)

**Fig. 5** Location of the Argonaut receiver in the worst-case experiment in Akureyri, Iceland, on December 19, 2017

from 12:15 on December 19, 2017 to 24:00 on December 19, 2017, GPST, with the same Rokubun receiver but at a higher latitude, i.e., Akureyri, northern Iceland, with high ionospheric scintillation. The receiver was located on a platform in the middle of buildings, which is a typical urban canyon environment, as shown in Fig. 5. The temporal evolution of the Rate Of Total electron content (TEC) Index (ROTI) during the experimental period at station AKUR, which is one of the stations provided by the National Land Survey of Iceland located at Akureyri University and which is only a few kilometers from the location of the receiver in our experiment, was calculated and compared with the ROTI of the International GNSS Service (IGS) station ZIMM, located in the mid-latitudes (Switzerland). The results are shown in Fig. 6, from which it is obvious that the ROTI of AKUR is higher than that of ZIMM, especially during the latter half of the experimental period, with the ROTI of AKUR reaching 2–3 times that of ZIMM. These findings are remarkable proof of the high ionospheric scintillation in this region (Pi et al. 1997; Tiwari et al. 2013; Aquino et al. 2005). All these conditions lead to a high possibility of cycle slips. The sampling rate was 5 Hz and the total number of measurements is greater than 1,500,000.

The histogram of the distribution of the DCV residuals between [− 6, 6] is presented in Fig. 7. Most of the values appear clustered in integer cycles, and clear boundaries are observed between clusters of different integer cycles. Such results strongly show that cycle slips can be not only detected but also repaired by correcting the corresponding integer number of wavelengths for epochs with *C*/*N*0 not smaller than 25. We should further mention that there is a small peak at −0.5 cycles; we surmise that this is attributable to undetected half-cycle ambiguities that were produced during the tracking process in the receiver (Lin and Yu. 2013).

Based on the above statistics, we can detect and repair the cycle slips using Eqs. (7–9). The threshold can be determined by the RMS values. For example, setting the threshold to 3 times of RMS should correctly repair the cycle slips with a probability of 99.73%. Considering that all the RMS values in different *C*/*N*0 intervals for the 5 Hz data are smaller than 0.08, we can set the threshold as 0.25 to ensure a very small probability of false alarms and missed detections, and to simultaneously avoid the influences of the abovementioned half-cycle ambiguities

## Comparative experiment with the high-end receiver

To study the difference in performance between low-cost and high-end receivers, we carried out a comparative experiment in static mode. The low-cost receiver was a u-blox receiver with NEO-M8T module, the high-end receiver was a Novatel Propak6. They were connected to the same

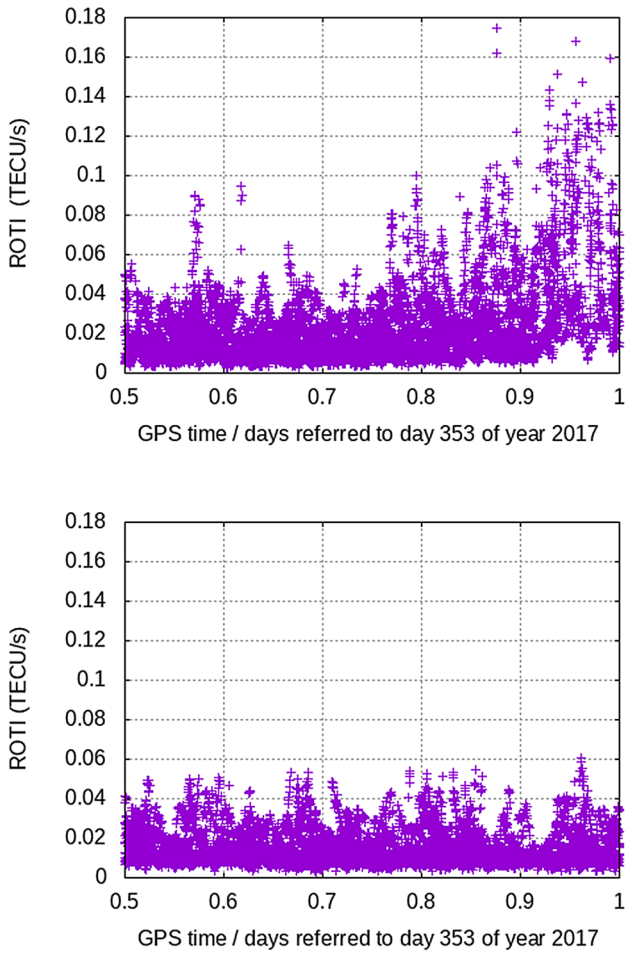


**Fig. 6** ROTI values of station AKUR (top) and station ZIMM (bottom) during the experimental period

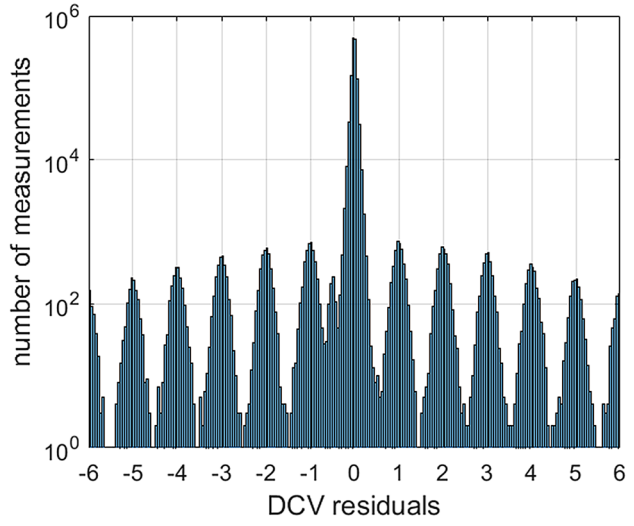


**Fig. 7** Histogram of the distribution of the DCV residuals of the 5 Hz static data collected from Akureyri, Iceland, on December 19, 2017, with the Argonaut receiver ($C/N0 \geq 25$, in cycles)

antenna installed on the roof of the building of Aerospace Information Research Institute in Beijing, China. The static observations of these two receivers were collected for 2 days with sampling rate of 10 Hz. We generated data with different intervals and calculated the RMS values of the DCV residuals. The results are shown in Table 4 and Fig. 8 and indicate that the RMS values show an almost linear trend for both receivers. However, the value of the slope for the u-blox receiver is more than twice that for the Novatel receiver. These results show that for the u-blox single-frequency receivers, although the RMS values and slope are larger than those of high-end receivers, the DACS-DR method can also be used to detect and repair cycle slips reliably when the sampling interval is not longer than 0.5 s.

## LLI performance

The LLI provided by receivers reflects the condition of cycle slips. According to the Receiver Independent Exchange Format (RINEX) format, 2 bits are allocated to this indicator, the occurrence of a cycle slip is detected when the LLI is set to bit 0, whereas the LLI is set to bit 1 when the presence of a half-cycle slip is suspected for some squaring-type receiver. The data set collected from Iceland with frequent cycle slips can provide a visual understanding of the performance of the LLI. The histogram of the distribution of the DCV residuals with LLI = 0, i.e., the LLI marked cycle slips have been removed, is illustrated in Fig. 9 for the cycle interval of [−6, 6]. We can see that most observations with the DCV residuals larger than 1, which means cycle slips occur, have been removed, although some obvious cycle slips remain with large DCV residuals that were not detected by the LLI. The histogram of the distribution of the DCV residuals with LLI ≠ 0, i.e., suspected cycle slips were detected by the receiver, is presented in Fig. 10 for the cycle interval of [−6, 6]. Most of the DCV residuals appear clustered in cycles at integers other than zero, indicating with a high probability that the cycle slips are correctly detected with LLI. In contrast, the residuals clustered around zero likely represent the cycle slips incorrectly marked by the LLI.

We also compared the cycle slips detection results between the LLI and the DACS-DR method with this static data set. We set the threshold as 0.25 cycles, which can ensure a very small probability of false alarms and missed detections while simultaneously avoiding the influences of half-cycle ambiguities. The confusion matrix shown in Table 5 compares the numbers of cycle slips detected by these two approaches.

Table 5 shows that for the measurements with $C/N0 \geq 25$, 14,370 cycle slips were detected by both the LLI and DACS-DR method. A total of 1916 of the measurements in which the absolute values of the DCV

**Table 4** RMS values of the u-blox receiver and the Novatel receiver for different sampling intervals (in cycles)

| Receiver | Interval(s) | | | | | | |
|---|---|---|---|---|---|---|---|
| | 0.1 | 0.2 | 0.5 | 1 | 2 | 5 | 10 |
| u-blox | 0.020 | 0.041 | 0.097 | 0.203 | 0.484 | 1.252 | 2.417 |
| Novatel | 0.013 | 0.021 | 0.048 | 0.096 | 0.192 | 0.503 | 1.097 |

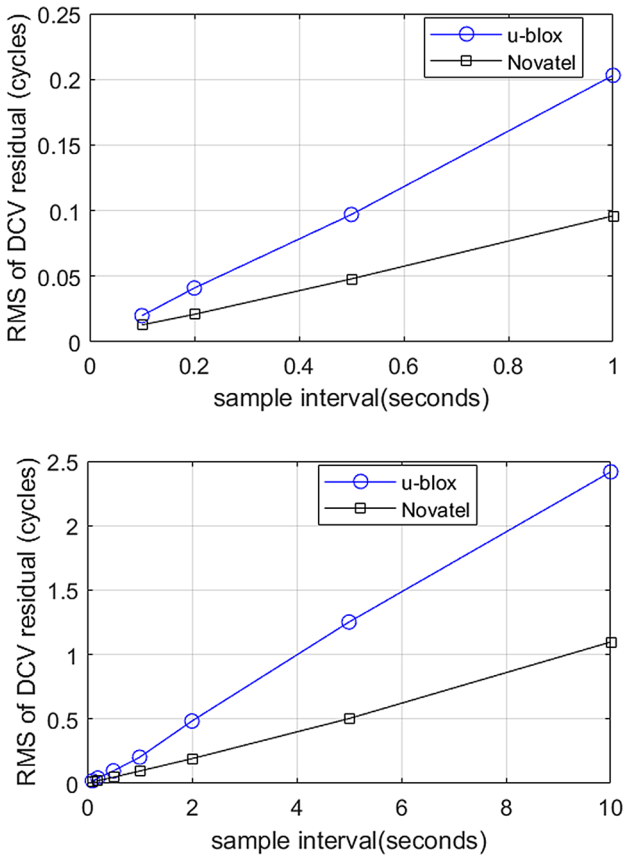


**Fig. 8** Comparison of the RMS values between the u-blox receiver and Novatel receiver for different sampling intervals (in cycles)

residuals were larger than 0.25 were marked as having no cycle slips by the LLI. At the same time, 23,633 of the measurements were marked as having cycle slips by the LLI but were not detected by the DACS-DR method. These results demonstrate that it is possible for the LLI of the u-blox NEO M8T to indicate cycle slips incorrectly, thereby decreasing the number of available measurements or omitting the real cycle slips. In addition, we notice that the number of cycle slips marked by the LLI but not detected by the DACS-DR method is very large. The reason for this discrepancy is that during the periods when it is easy to produce cycle slips, i.e., usually at the beginning of tracking a signal or when the *C*/*N*0 is particularly low, the receiver systematically marks all the data with a cycle slip flag.

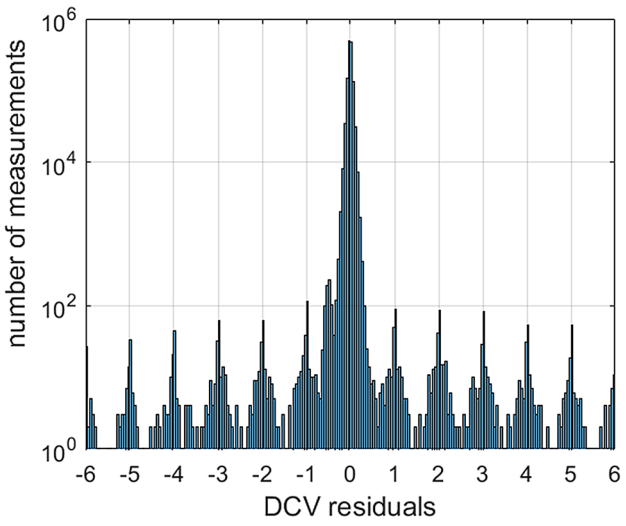


**Fig. 9** Histogram of the distribution of the DCV residuals in which LLI = 0 for the 5 Hz static data collected from Akureyri, Iceland, on December 19, 2017, with the Argonaut receiver, ($C/N0 \geq 25$, in cycles)

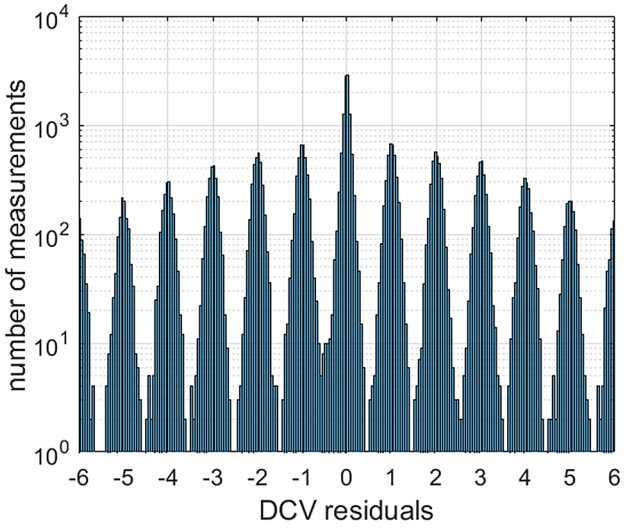


**Fig. 10** Histogram of the distribution of the DCV residuals in which LLI ≠ 0 for the 5 Hz static data collected from Akureyri, Iceland, on December 19, 2017, using the Argonaut receiver ($C/N0 \geq 25$, in cycles)

**Table 5** Confusion matrix of the numbers of cycle slips (CS) detected by the LLI and DACS–DR method, using the static data collected with the Argonaut receiver ($C/N0 \geq 25$)

| $C/N0 \geq 25$ | LLI | |
|---|---|---|
| | CS | No CS |
| DACS-DR | | |
| CS | 14,370 | 1916 |
| No CS | 23,633 | – |

## Positioning experiment

According to the analyses presented above, the DACS-DR method can not only detect but also repair cycle slips reliably at a high sampling rate for a low-cost single-frequency receiver. In this way, increases in the number of available measurements and the continuity of positioning are obtained, with an expected positioning improvement.

To validate the performance improvement of positioning by using the DACS-DR method, the worst-case data set used in the previous section were selected to perform a precise positioning experiment. The kinematic PPP method with float ambiguity estimation (Gill et al. 2017) was selected to solve the coordinates of the receiver. The data processing software was modified based on the open-source program package RTKLIB (Takasu 2013), which supports real-time and post-processing positioning models. The processing strategy for the observation error sources for single-frequency PPP is listed in Table 6.

The static-PPP method was used to generate the reference coordinates to evaluate the kinematic positioning accuracy. All data spanning 12 h were used to estimate the receiver coordinates to ensure sufficient convergence. The last coordinates estimated from the static-PPP filter were used as reference coordinates.

The cut-off values for the elevation and $C/N0$ were set as 8° and 25, respectively. Only GPS data were collected and used in this experiment. The number of tracked satellites ranged from 4 to 9. As the results of insufficient satellites and frequent cycle slips, the solution convergence with difficulty and the ambiguity parameters reinitialized frequently. Based on the analyses presented above, the threshold of the DCV residuals to detect cycle slips was set to 0.25 cycles. For the repair of cycle slips, to use as many of the available measurements as possible, the threshold was set to 0.5 for measurements with absolute values of DCV residuals larger than 1 cycle. The threshold was set to 0.25 for data with absolute values of the DCV residuals smaller than 1 cycle (half-cycle slips were also repaired with a threshold of 0.25).

The PPP solution from two representative data subsets corresponding to two time intervals are shown in Figs. 11 and 12 to intuitively illustrate the results. In these two figures, the blue lines represent the positioning error with cycle slips detected by the LLI, while the red line represents the positioning error using the DACS-DR method to detect and repair the cycle slips.

Figure 11 demonstrates that the positioning error with the DACS-DR method during the convergence process was smaller than that with the LLI. Moreover, some of the large jumps were also avoided with the DACS-DR method. The same can be concluded from Fig. 12. In addition, obviously, four re-convergences occurred for the blue line between 19:30 and 19:55 because some of the carrier phase observations jumped in the same epoch. These re-convergence events disappeared for the red line corresponding to the DACS-DR method.

We also report the results of all data periods, which can convergence (approximately 5 h of data in total). The distributions of the positioning error corresponding to the reference coordinates are presented in Fig. 13, and the RMS values are listed in Table 7. Figure 13 reveals that compared with the positioning error distributions obtained with the LLI for detecting cycle slips (upper row of panels), the bottom panels present more concentrated distributions that reflect fewer large errors in the positioning results obtained with the DACS–DR method. Table 7 shows that the RMS values of the positioning error using the LLI to detect cycle slips on the east, north and vertical components are 3.07, 5.14 and 15.95 m, respectively, while the values corresponding to the DACS-DR method on these three components are 1.71, 2.87 and 12.57 m, respectively. The RMS improved by 44.2% and 21.2% in the horizontal and vertical direction, respectively, for the DACS-DR method compared with the positioning results obtained with the LLI to detect cycle slips. The error on the vertical component is large due to poor geometry in this direction caused by the obstruction of the surrounding buildings. Although the absolute accuracy is not high due to the lack of satellites, the serious multipath,

**Table 6** Processing strategy for the kinematic single-frequency PPP experiment

| Errors and model | Settings |
|---|---|
| Satellite orbit and clock error | IGS final orbit and clock products (CDDIS-IGS 2020) |
| Ionosphere error | IGS final GIM products (CDDIS-IGS 2020) |
| Troposphere error | Estimated the zenith delay of the wet troposphere |
| Sagnac and relativistic effects | Estimation model recommended by IS-GPS-200 (ICD 2013) |
| Other estimated parameters | Receiver coordinates, receiver clock error, integer ambiguities |
| Weight model | $C/N0$ and sigma weight model in (Wieser and Brunner 2000) |

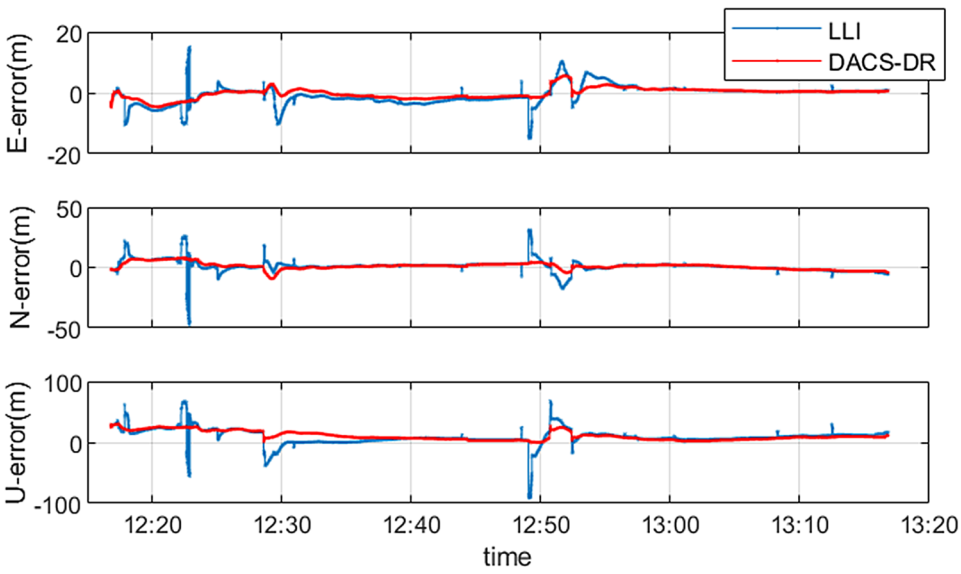


**Fig. 11** Time series of the positioning error for the east, north and vertical components for the period from 12:16 to 13:16. Data were collected from Akureyri, Iceland, on December 19, 2017, with the Argonaut receiver

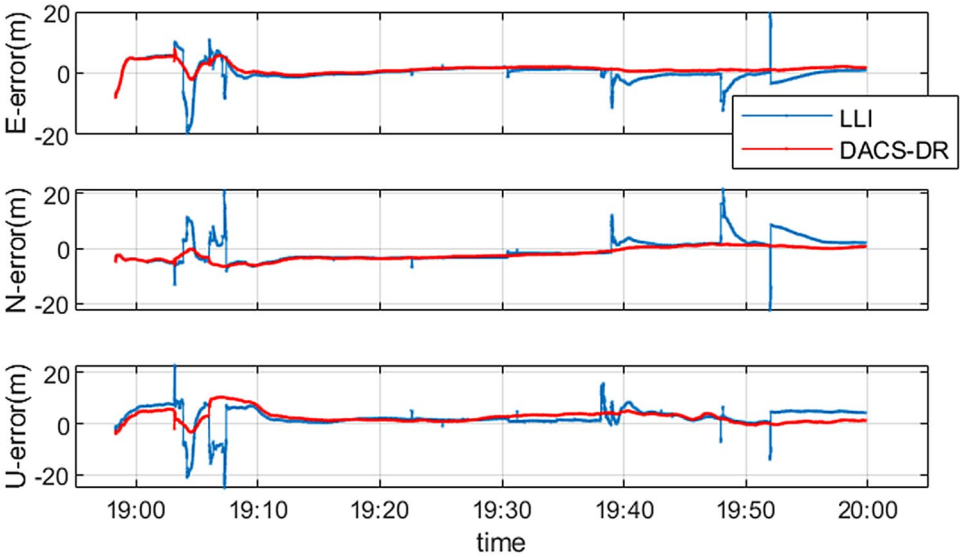


**Fig. 12** Time series of the positioning error on the east, north and vertical components for the period from 18:58 to 20:00. Data were collected from Akureyri, Iceland, on December 19, 2017, with the Argonaut receiver

and the frequent data interruptions in this poor environment, the results still show great improvement in the positioning performance.

## Conclusion

Cycle slip is an important source of error that deserves considerable attention, especially in precise positioning technologies such as PPP and RTK. Undetected cycle slips or excessive numbers of simultaneous cycle slips will produce unknown biases in the positioning results and decrease both the continuity and the reliability of the positioning endeavor. Fortunately, Doppler measurements are immune to cycle slips and the Doppler-aided method benefits from an increase in the sampling rate. However, studies in this field are either lacking research with high-rate data or are based on insufficient data set. This study presents likely the first systematic analysis of the DCV residuals with different sampling rates under static and kinematic modes for low-cost single-frequency receivers and reports a discussion on the reliability of the LLI provided by the receiver with u-blox M8T module. The geometry-free DACS-DR method, which is simple, efficient and reliable for single-frequency receivers with high-rate observations, was introduced in this contribution to deal with the problem of cycle slips.

We concluded that the DCV residuals are correlated with $C/N0$ and obey zero-mean normal distribution. For the 5 Hz and 10 Hz data, the RMS values are no more than 0.08 and 0.12 under static and kinematic modes, respectively. These

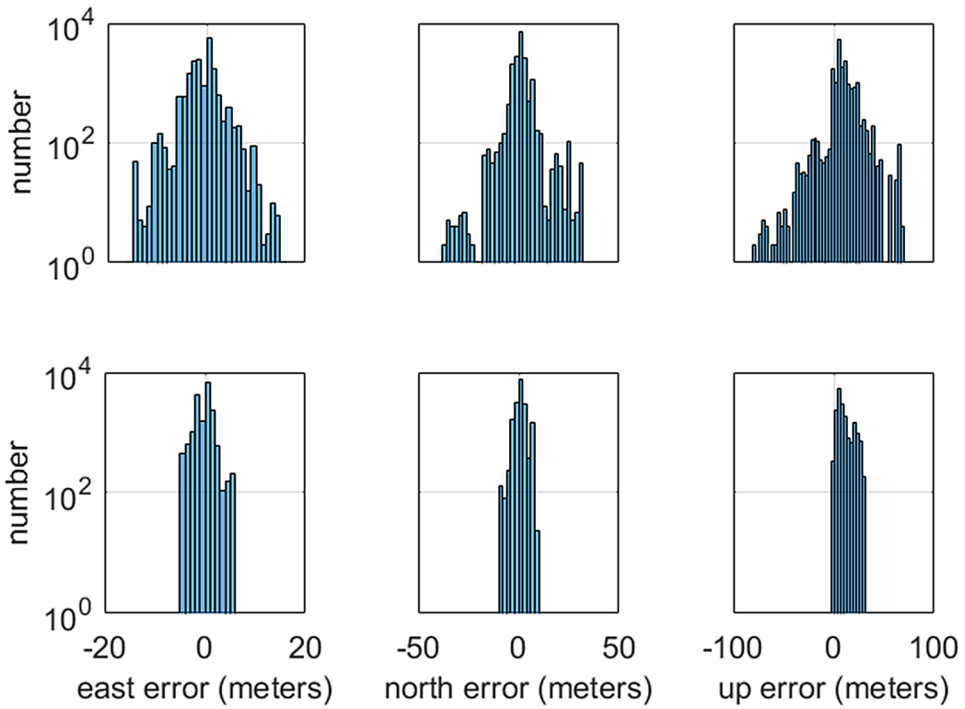


**Fig. 13** Distribution of the difference between the reference coordinates and the estimated coordinates based on different cycle slip processing methods for all data collected from Akureyri, Iceland on December 19, 2017, with the Argonaut receiver. Top row: LLI; bottom row: DACS-DR method

values give us a reference to determine the thresholds in the DACS-DR method. We also found that the LLI is sometimes not reliable, so it can be replaced by a more efficient and reliable technique, such as the DACS-DR method when the high sampling rate is available.

The float-PPP results based on the data set collected at a location with severe building obstructions and a typical high ionospheric scintillation clearly showed an improvement in the performance with the proposed DACS-DR method based on 5 Hz data. The results demonstrated that the convergence time, large jumps, and the number of re-convergence events were all reduced with this method. Moreover, the RMS values of the positioning error in the horizontal and vertical directions improve by 44.2% and 21.2%, respectively, compared with the positioning results using the LLI to detect the cycle slips

In this study, the float-PPP technique was used to validate the proposed method. It is obvious that the proposed method can also be helpful in other applications in which cycle slips need to be addressed under high-rate GNSS data.

**Acknowledgements** This work was partially supported by the National Key Research Program of China (No. 2017YFE0131400), the National Natural Science Foundation of China (No.41674043, 41704038, 41730109), Beijing Nova program (xx2017042) and Young Top-Notch Talents Team Program of Beijing Excellent Talents Funding (2017000021223ZK13), Strategic Priority Research Program of the Chinese Academy of Sciences (No. XDA17010304, XDA17010200), Beijing Natural Science Foundation (8184092) and CAS Pioneer Hundred Talents Program. Thanks to the National Land Survey of Iceland and IGS for the free data of stations AKUR and ZIMM. The second author acknowledges the continuous support of his family, which facilitated and motivated the performance of the high-latitude low-cost experiment during his private visit to his son David at Akureyri.

**Table 7** RMS values of the positioning error on the three components for the data collected from Akureyri, Iceland, on December 19, 2017, with the Argonaut receiver (in m)

| | East | North | Up |
|---|---|---|---|
| LLI | 3.07 | 5.14 | 15.95 |
| DACS-DR | 1.71 | 2.87 | 12.57 |

## References

Aquino M, Moore T, Dodson A, Waugh S, Souter J, Rodrigues FS (2005) Implications of ionospheric scintillation for GNSS users in Northern Europe. J Navig 58(2):241–256

Banville S, Langley RB (2012) Cycle-slip correction for single-frequency PPP. In: Proc. ION GNSS 2012, Institute of Navigation, Nashville, Tennessee, USA, September 17–21, pp 3053–3061

Bastos and Landau (1988) Fixing cycle slips in dual-frequency kinematic GPS-applications using Kalman filtering. Manuscr Geod 13(4):249–256

Bisnath SB, Langley RB (2000) Efficient, automated cycle-slip correction of dual-frequency kinematic GPS data. In: Proc. ION GPS 2000, Institute of Navigation, Salt Lake City, UT, USA, September 19–22, pp 145–154

Blewitt G (1990) An automatic editing algorithm for GPS data. Geophys Res Lett 17(3):199–202

Carcanague S (2012) Real-time geometry-based cycle slip resolution technique for single frequency PPP and RTK. In: Proc. ION GNSS 2012, Institute of Navigation, Nashville, Tennessee, USA, September 17–21, pp 1136–1148

CDDIS-IGS (2020). ftp://cddis.gsfc.nasa.gov/pub/gps/products/. Accessed 6 June 2020
Cederholm P, Plausinaitis D (2014) Cycle slip detection in single frequency GPS carrier observations using expected Doppler shift. Nord J Surv Real Estate Res 10(1):63–79
Chen W, Hu C, Gao S, Chen Y, Ding X (2009) Error correction models and their effects on GPS precise point positioning. Surv Rev 41(313):238–252
Choy S (2011) High accuracy precise point positioning using a single frequency GPS receiver. J Appl Geodesy 5(2):59–69
Collin and Warnant (1995) Application of wavelet transform for GPS cycle slip correction and comparison with Kalman Filter. Manuscr Geod 20:161–172
Dai Z (2012) MATLAB software for GPS cycle-slip processing. GPS Solut 16(2):267–272
Dai Z, Knedlik S, Loffeld O (2009) Instantaneous triple-frequency GPS cycle-slip detection and repair. Int J Navig Obs. https://doi.org/10.1155/2009/407231
Gill M, Bisnath S, Aggrey J, Seepersad G (2017) Precise point positioning (PPP) using low-cost and ultra-low-cost GNSS receivers. In: Proc. ION GNSS 2017, Institute of Navigation, Portland, Oregon, USA, September 25–29, pp 226–236
Hernández-Pajares M, Juan JM, Sanz J, Aragón-Àngel À, García-Rigo A, Salazar D, Escudero M (2011) The ionosphere: effects, GPS modeling and the benefits for space geodetic techniques. J Geodesy 85(2):887–907
Hernández-Pajares M, Roma-Dollase D, Garcia-Fernàndez M, Orus-Perez R, García-Rigo A (2018) Precise ionospheric electron content monitoring from single-frequency GPS receivers. GPS Solut 22(4):102
Hofmann-Wellenhof B, Lichtenegger H, Collins J (2012) Global positioning system: theory and practice. Springer, Vienna
ICD G (2013) Global Positioning Systems Directorate System Engineering & Integration Interface Specification. IS-GPS-200H Navstar GPS Space Segment/Navigation User Interfaces
IGS R-S (2015) RINEX-The Receiver Independent Exchange Format (Version 3.03). ftp://igs.org/pub/data/format/rinex303.pdf
Kirkko-Jaakkola M, Traugott J, Odijk D, Collin J, Sachs G, Holzapfel F(2009) A RAIM approach to GNSS outlier and cycle slip detection using L1 carrier phase time differences. In: Proc. 2009 IEEE workshop on signal processing systems, Tampere, Finland, October 7–9, pp 273–278
Kleusberg A, Georgiadou Y, van den Heuvel F, Héroux P (1993) GPS data preprocessing with DIPOP 3.0. Internal technical memorandum, Department of Surveying Engineering, University of New Brunswick, Fredericton
Li B, Liu T, Nie L, Qin Y (2019) Single-frequency GNSS cycle slip estimation with positional polynomial constraint. J Geodesy 93(9):1781–1803
Lichtenegger H, Hofmann-Wellenhof B (1990) GPS-data preprocessing for cycle-slip detection. In: Proc. global positioning system: an overview. International Association of Geodesy Symposia, New York, USA, September 10–13, pp 57–68
Lin SG, Yu FC (2013) Cycle slips detection algorithm for low-cost single-frequency GPS RTK positioning. Surv Rev 45(330):206–214
Parkinson BW, Enge P, Axelrad P, Spilker JJ Jr (1996) Global positioning system: theory and applications, vol II. American Institute of Aeronautics and Astronautics, Washington
Pi X, Mannucci A, Lindqwister U, Ho C (1997) Monitoring of global ionospheric irregularities using the worldwide GPS network. Geophys Res Lett 24(18):2283–2286
Ren Z, Li L, Zhong J, Zhao M, Shen Y (2011) A real-time cycle-slip detection and repair method for single frequency GPS receiver. Int Proc Comput Sci Inf Technol 17:224–230
Takasu T (2013) RTKLIB: an open source program package for GNSS positioning. Software and documentation. http://www.rtklib.com/. Accessed 6 June 2020
Tiwari R, Strangeways H, Tiwari S, Ahmed A (2013) Investigation of ionospheric irregularities and scintillation using TEC at high latitude. Adv Sp Res 52(6):1111–1124
Wang Y (2019) Precise localization in urban Area. Dissertation, University of Toulose
Wang L, Li Z, Ge M, Neitzel F, Wang X, Yuan H (2019) Investigation of the performance of real-time BDS-only precise point positioning using the IGS real-time service. GPS Solut 23(3):66
Wieser A, Brunner FK (2000) An extended weight model for GPS phase observations. Earth Planets Sp 52(10):777–782
Wu Y, Jin S, Wang ZM, Liu JB (2010) Cycle slip detection using multi-frequency GPS carrier phase observations: a simulation study. Adv Sp Res 46(2):144–149
Xu G, Xu Y (2007) GPS: theory, algorithms and applications. Springer, Vienna
Zhang X, Li P (2016) Benefits of the third frequency signal on cycle slip correction. GPS Solut 20(3):451–460
Zhao Q, Sun B, Dai Z, Hu Z, Shi C, Liu J (2015) Real-time detection and repair of cycle slips in triple-frequency GNSS measurements. GPS Solut 19(3):381–391



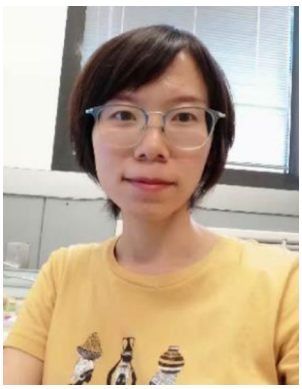

**Jiaojiao Zhao** is currently an engineer and a doctoral student at Aerospace Information Research Institute (AIR), Chinese Academy of Sciences (CAS) and a visiting scholar at Universitat Politècnica de Catalunya (UPC). Her current research activities are related to GNSS data processing strategies for precise positioning and integrity monitoring.

**Manuel Hernández-Pajares** is a Full Professor at Universitat Politècnica de Catalunya (UPC), Barcelona, Spain. Since 1994 he has focused on new algorithms for precise ionospheric sounding and GNSS navigation. He has been the chair of the International GNSS Service (IGS) Ionosphere WG (2002–2007). He created the new research group, UPC-IonSAT, in Nov. 2013, and presently belongs as well to the IEEC-CTE research group.

**Zishen Li** is currently an associate professor at AIR, CAS and the leader of the research group on GNSS remote sensing and precise positioning. He received his Ph.D. degree in Geodesy and Surveying Engineering from the Institute of Geodesy and Geophysics (IGG), CAS in 2013. His current activates related to the real-time ionospheric remote sensing and correction for various GNSS applications.

**Liang Wang** is currently a postdoctoral researcher at AIR, Chinese Academy of Sciences (CAS). He received the Ph.D. degree in Signal and Information Processing from the University of Chinese Academy of Sciences in 2019. His current research activities are related to the multi-GNSS real-time precise positioning and data processing.

**Hong Yuan** received his Ph.D. degree from Shanxi Astronomy Observatory, CAS in 1995, and is currently a professor and the director of the Navigation System Department at AIR, CAS. His interest currently focuses on ionospheric modeling and multi-sensor-based navigation.